Synthesis and Characterization of Sn/R, Sn/Si−R, and Sn/SiO_2 Core/Shell Nanoparticles

Chung-Sung Yang, Qi Liu, and Susan M. Kauzlarich*

Department of Chemistry, University of California, One Shields Avenue, Davis, California 95616

Brian Phillips

Department of Chemical Engineering and Materials Science, University of California, One Shields Avenue, Davis, California 95616

Received August 16, 1999

Nanometer-sized tin, Sn/R, and Sn/Si−R (R = n-C_4H_9), core/shell nanoparticles have been prepared by the reaction of $SnCl_4$ or $SiCl_4$ with Mg_2Sn in ethylene glycol dimethyl ether (glyme) and subsequently with n-C_4H_9Li. Sn/SiO_2 core/shell nanoparticles are produced from the reaction of Mg_2Sn with $SiCl_4$ and subsequent reaction with H_2O_2. Fourier transform Infrared (FTIR) spectra are consistent with *n*-butyl surface termination for the *n*-butyl-capped tin (Sn/*n*-butyl) and the silicon-*n*-butyl capped tin (Sn/Si-*n*-butyl) core/shell nanoparticles. High-resolution transmission electron microscope (HRTEM) confirms that the core part of Sn/*n*-butyl and Sn/Si- *n*-butyl nanoparticles is consistent with the tetragonal structure of tin, exhibiting lattice fringes of the {200} crystal plane (2.92 Å). The FTIR spectrum of Sn/SiO_2 confirms the evidence of silica capping and selected area electron diffraction (SAED) is consistent with an amorphous shell (SiO_2) and crystalline Sn core. Solid-state nuclear magnetic resonance (NMR) spectra and X-ray powder diffraction (XRD) pattern provide supporting evidence for the tetragonal structure of β-tin as the core part of Sn/SiO_2 nanoparticles. The typical size distribution of Sn/*n*-butyl, Sn/Si-*n*-butyl, and Sn/SiO_2 nanoparticles (diameter) range from 7 to 15 nm derived from TEM micrographs. The average radius ratio (Rr) value, (radius of SiO_2/radius of Sn) for Sn/SiO_2 derived from 24 individual nanoparticles in TEM images is 0.17 (0.02).

Introduction

Metallic nanoparticles as well as semiconductor quantum dots have attracted much attention for the past decade.[1−3] Clusters and aggregates of atoms in the nanometer range display properties that are distinct from either simple molecules or bulk materials. As the diameter of the particle reaches the nanometer scale, quantum confinement effects are exhibited.[1,4,5] The exploitation of the unusual physical properties exhibited by these types of materials has captured the imagination of scientists and there is a great deal of ongoing research aimed at the development and utilization of nanotechnology. Applications of Sn nanoparticles are in the preparation of metal films,[6] as Li alloy anodes for rechargeable batteries,[7−9] and as precursors to SnO_2 nanoparticles for use as gas sensors.[3,10]

In this paper, we report a novel solution route to produce Sn/R, Sn/Si−R, and Sn/SiO_2 core/shell nanoparticles, where R = n-C_4H_9. This synthesis utilizes reactive Zintl salts and is performed at low temperatures. The Sn/Sn-n-C_4H_9 and Sn/Si-n-C_4H_9 offers a model to study the effects of surface functionalization with metal cores and semiconductor or insulator caps. The silica sphere of Sn/SiO_2 can offer a temporarily protective and porous surface before the tin nanoparticle is exposed to an oxidizing gas. It also provides a surface that is chemically assessable and well-known for its physical properties. This work builds on our previous work on Si and Ge nanoclusters with functionalized surfaces.[11−15] This paper presents the first example of

(1) Stella, A.; Nisoli, M.; Silvestri, S. D.; Svelto, O.; Lanzani, G.; Cheyssac, P.; Kofman, R. *Phy. Rev. B* **1996**, *53*, 15497.
(2) Sheng, H. W.; Lu, K.; Ma, E. *Acta Mater.* **1998**, *46*, 5195.
(3) Nayral, C.; Ould-Ely, T.; Maisonnat, A.; Chaudret, B.; Fau, P.; Lescouzères, L.; Peyre-Lavigne, A. *Adv. Mater.* **1999**, *11*, 61.
(4) Zang, S. B.; Zunger, A. *Appl. Phys. Lett* **1993**, *63*, 1399.
(5) Zhao, X.; Schoenfield, O.; Kumuro, S.; Aoyagi, Y.; Sugano, T. *Phys. Rev. B* **1994**, *50*, 18654.
(6) Cardenas-Triviño, G.; Alvial J.; M.; Klabunde, K. J.; Pantoja, M. O.; Soto, Z. H. *Colloid Polym. Sci.* **1994**, *272*, 310.
(7) Yang, J.; Winter, M.; Besenhard, J. O. *Solid State Ionics* **1996**, *90*, 281.
(8) Idota, Y.; Kubota, T.; Matsufuji, A.; Maekawa, Y.; Miyasaka, T. *Science* **1997**, *276*, 1395.
(9) Huggins, R. A. *Solid State Ionics* **1998**, *113*, pp57.
(10) Ihokura, K.; Watson, J. *The Stannic Oxide Gas Sensor-Principles and Applications*; CRC Press: Boca Raton, FL, 1994.
(11) Bley, R. A.; Kauzlarich, S. M. *J. Am. Chem. Soc.* **1996**, *118*, 12461.
(12) Yang, C.-S.; Kauzlarich, S. M.; Wang, Y. C. *Chem. Mater.* **1999**, *11*, 3666.
(13) Taylor, B. R.; Kauzlarich, S. M.; Lee, H. W. H.; Delgado, G. R. *Chem. Mater.* **1998**, *10*, 22.
(14) Taylor, B. R.; Kauzlarich, S. M.; Delgado, G. R.; Lee, H. W. H. *Chem. Mater.* **1999**, *11*, 2493.
(15) Yang, C.-S.; Kauzlarich, S. M.; Lee, H. W. H.; Delgado, G. R. *J. Am. Chem. Soc.* **1999**, *121*, 5191.

10.1021/cm990529z CCC: $19.00
Published on Web 03/09/2000

Scheme 1. Solution Synthesis Route for Sn/SiO_2 Core/Shell Nanoparticles.

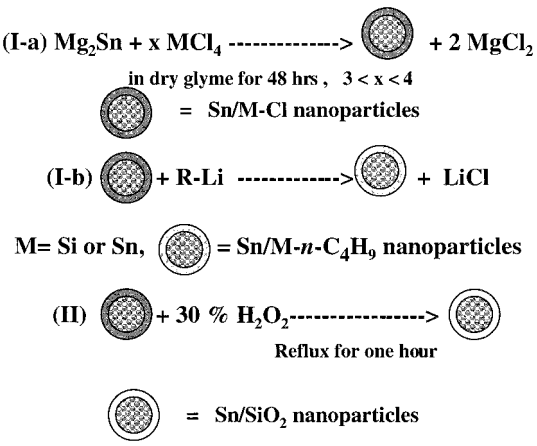

surface-capped and organic-functionalized tin nanoparticles.

Experimental Section

Materials. Magnesium flake (99.9%) was obtained from Strem Chemical. Tin powder (99.99%) was purchased from Johnson Matthey Company. Semiconductor grade $SiCl_4$ (99.99%, Aldrich) and $SnCl_4$ (99.995%, Aldrich) were used without further purification. Reagent-grade ethylene glycol dimethyl ether (glyme) (99.5%, Aldrich) was dried by stirring with potassium overnight and distilled under argon. Hydrogen peroxide 30% (Fisher scientific), ethyl alcohol 100% (Gold Shield chemicals), and the lithium reagent, n-C_4H_9Li (2.5 M, Aldrich), were used as supplied. All reagents and materials were handled either in nitrogen-filled drybox or with a Schlenk line using standard anaerobic techniques.

Synthesis. Mg_2Sn was synthesized by reacting stoichiometric amounts of Mg with Sn powder at 650 °C for 3 days in a sealed Nb tube which was then sealed in a quartz ampule filled with 0.25 atm argon.[16] The product displayed a metallic luster with dark gray color and was characterized by X-ray powder diffraction. The experimental diffraction pattern agrees with the calculated anti-fluorite structure for Mg_2Sn.[16,17]

Tin nanoparticles were produced from the reaction of 300 mg of Mg_2Sn (1.8 mmol) in 50 mL of glyme with 6.3 mmol $SiCl_4$ (0.72 mL) or $SnCl_4$ (0.73 mL), as shown in Scheme 1, step I-a. The solution was refluxed for 48 h under dry, deoxygenated argon. The Mg_2Sn gray powder does not dissolve in glyme and does not change its color during the reflux with $SiCl_4$. However, the gray powder does dissolve gradually in the reflux with $SnCl_4$. After 48 h refluxing, the mixture is allowed to cool to room temperature, and the solvent is removed via vacuum. New glyme solvent and n-butyllithium (2.5 mL) were added and stirred overnight to terminate the surface from silicon-chloride to silicon-n-butyl, as shown in Scheme 1, step I-b. Instead of functionalizing the surface, the other route is to produce Sn/SiO_2 as follows. The product synthesized from step I was refluxed with H_2O_2 (30%) for 1 h to oxidize the silicon-chloride surface to silica (SiO_2), Scheme 1, step II. After termination or oxidation of the surface, the solvent was removed in vacuo. A mixture of nanoparticles and salt were left as a solid residue. In the case of the alkyl-terminated surface, hexane was added to the solids. The solution was transferred to a separatory funnel, and deionized water was added several times to remove the salts. The Sn/SiO_2 nanoparticles precipitated from solution upon addition of water and the solid was washed with water several times. The deep green (Sn/n-C_4H_9), gray (Sn/Si-n-C_4H_9), or black (Sn/SiO_2) nanoparticles were precipitated from the solution. The product can be dried as a powder or partially resuspended in 100% ethanol. However, even the alkyl-terminated nanoparticles tend to precipitate out of solution after a period of time. The products appear to be both air and moisture stable. The conditions of surface termination and weights of the products are provided in Table 1.

Table 1. Conditions of Surface Termination and Product Weight

reaction no.	wt (mg) of Mg_2Sn	surface termination	product wt (mg)
1: $Mg_2Sn + SnCl_4$	299.1	$-n$-C_4H_9	171.7
2: $Mg_2Sn + SiCl_4$	300.6	$-n$-C_4H_9	197.5
3: $Mg_2Sn + SiCl_4$	300.9	$-SiO_2$	262.3

Characterization. X-ray powder diffraction data of Mg_2Sn were obtained by using an Enraf-Nonius Guinier camera equipped with a quartz monochromator. A Siemens D500 powder diffractometer was used to collect data on Sn nanoparticles. All X-ray powder diffraction were collected with 0.02° − 2θ step and 15-s count. The size of the particles was determined from the width of the reflections according to the Scherrer equation[18] using Si (111) (NBS standard) as a standard. The diffractometer instrumental line width was also calibrated using LaB_6 (NBS) as a standard. The samples were prepared as powders on a zero-background sample holder. HRTEM samples were prepared by evaporating the colloids onto lacey carbon-coated electron microscope 200-mesh grid. Selected area diffraction was obtained for all samples and matched the pattern expected for crystalline β-tin. The electron microscopes are Philip CM300 UT/FEG HRTEM operating with a 300-keV accelerating voltage and Topcon 002B with a 200-keV accelerating voltage at the National Center for Electron Microscopy (NCEM). FTIR spectra were obtained at room temperature by dropping the ethanol colloid on a CsI plate and allowing the solvent to evaporate. The ^{119}Sn NMR spectra were obtained at 150.2 MHz with a Chemagnetics CMX 400 spectrometer using a standard MAS probe configured for 4-mm (outside diameter) rotors, but with a stationary (nonspinning) sample. For the spectrum of the metalic regions, a chemical shift echo sequence was used with pulse widths of 3 μs ($\pi/2$) and 6 μs (π) separated by a 40-μs interpulse delay, and a 20-ms relaxation delay for 160 000 acquisitions. The echo was digitized at 1 MHz and Fourier transformed from the echo maximum as origin. Frequency scale is relative to tetramethyltin ($\delta = 0$), referenced to an external sample of tetraphenyltin ($\delta = -117$ ppm). The absolute ^{119}Sn NMR intensity for the oxide component was measured by comparison of spin-echo intensity with that from samples of tetraphenyl tin ($\delta = -117$ ppm) and SnO_2 ($\delta = -600$ ppm). No background signal was observed from the sample probe/rotor assembly. Spin−echoes were generated with a $90-\tau-180$ acquire pulse sequence where the pulse lengths were 4 and 8 μs, respectively, and $\tau = 60$ μs. All intensities were measured after complete spin−lattice relaxation and corrected for spin−spin (T_2) relaxation effects. The MAS spectrum was taken with the sample spinning at 12.5 kHz using the same spin echo sequence, but with $\tau = 80$ μs, corresponding to one rotor period.

Results and Discussion

Mg_2Sn crystallizes in an anti-fluorite structure and can be synthesized directly from the elements. The product is produced in high yield from the elements as a deep gray powder with a slight metallic luster. Mg_2Sn is a compound that fits into the category of Zintl compounds.[19] In this formalism, the Mg is considered to be Mg^{2+}, and Sn, is therefore, formally, Sn^{4-}. How-

(16) Grosch, G. H.; Range, K.-J. *J. Alloy. Comput.* **1996**, *235*, 250.
(17) Dyuzheva, T. I.; Bendeliani, N. A.; Dzhavadov, L. N.; Kolobyanina, T. N.; Nikolaev, N. A. *L. Alloys Comput.* **1995**, *223*, 74.
(18) Cullity, B. D. *Elements of X-ray Diffraction*, 2nd ed.; Addison-Wesley: Menlo Park, CA, 1978.
(19) Kauzlarich, S. M. *Chemistry, Structure and Bonding of Zintl Phases and Ions*; VCH Publishers: New York, 1996.

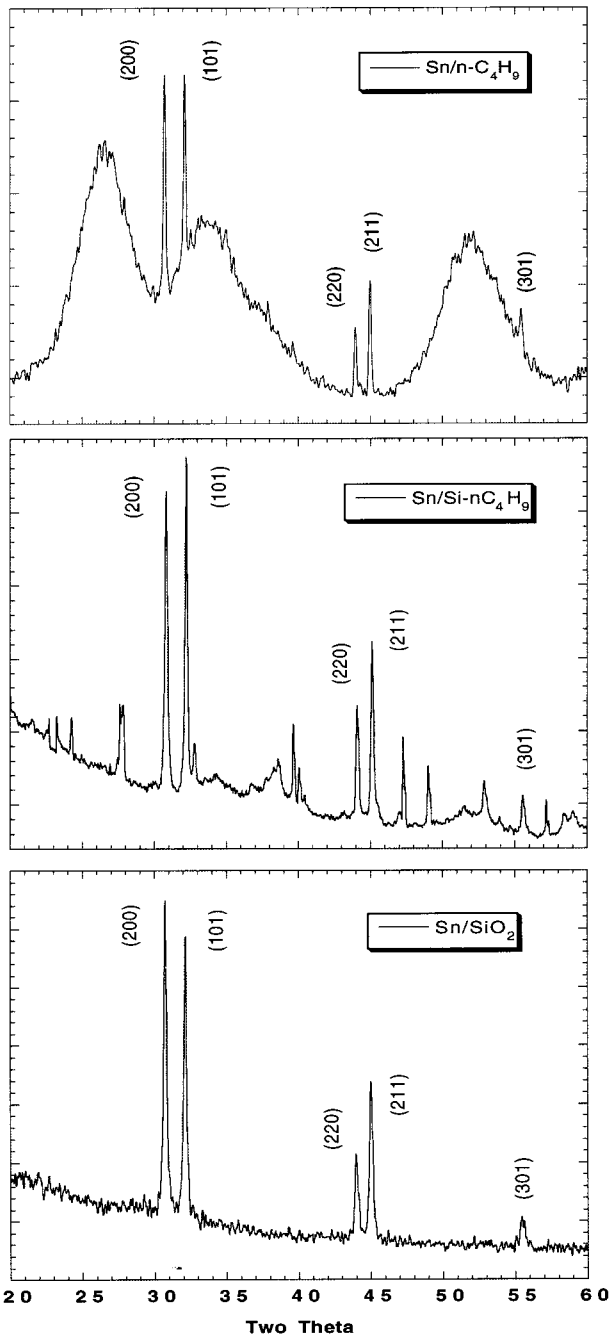

Figure 1. The X-ray powder diffraction of Sn/*n*-C_4H_9, Sn/Si-*n*-C_4H_9, and Sn/SiO_2 nanoparticles. The first five identified peaks match that of β-Sn (JCPDS 4-0673).

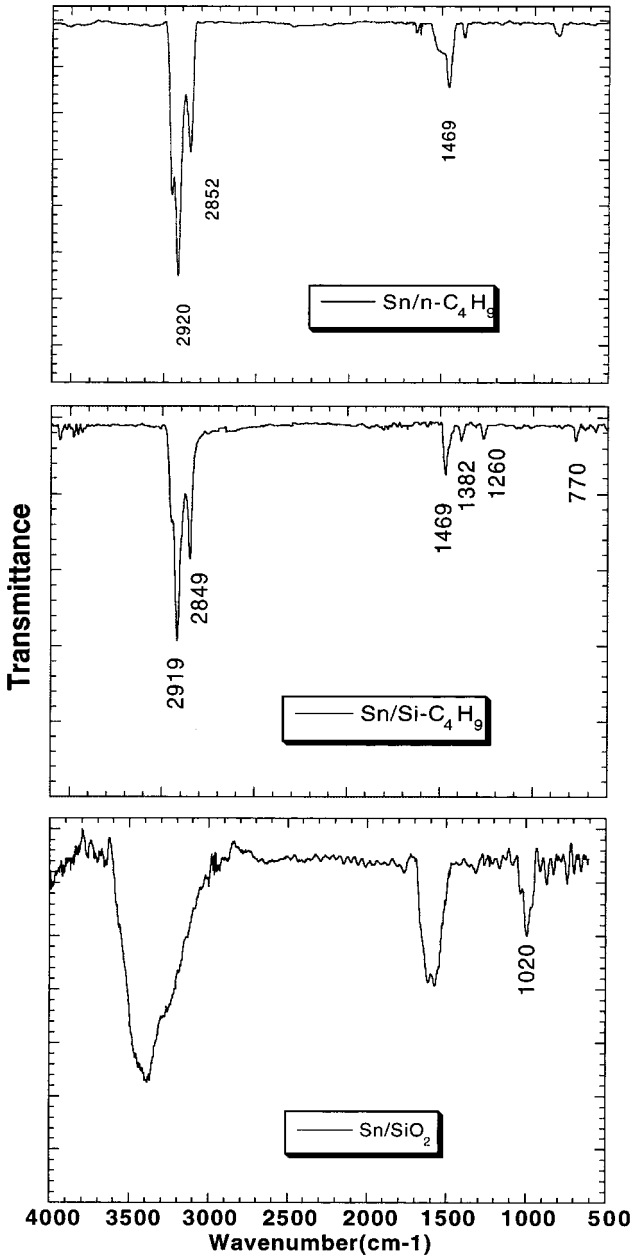

Figure 2. FT-IR spectra for Sn/-*n*-C_4H_9, Sn/Si-*n*-C_4H_9, and Sn/SiO_2 nanoparticles.

ever, the X-ray photoelectron spectroscopy (XPS) indicates that rather than being an ionic solid, this compound shows a great deal of covalency.[16] This paper employs Mg_2Sn as a starting reagent to produce Sn nanoclusters with various surface terminations. The choice of starting reagent follows from our previous work on the preparation of Si and Ge nanoclusters from the appropriate Mg_2E (E = Si, Ge). The reaction of Mg_2Sn with excess $SiCl_4$ or $SnCl_4$ presumably produces a surface terminated with −Cl[11,12,15] which offers chemical accessibility for oxidization by hydrogen peroxide or termination of the surface with alkyls. The yield of the Sn core/shell nanoparticles is ∼70%, on the basis of the weight of Mg_2Sn and product, as shown in Table 1. Once the solvent is removed, the product appears as a fine greenish, gray, and black colored powders for Sn/*n*-C_4H_9, Sn/Si-*n*-C_4H_9, and Sn/SiO_2, respectively. The products, Sn/*n*-C_4H_9 and Sn/Si-*n*-C_4H_9 can be resuspended in hexane and the product, Sn/SiO_2, can be resuspended in ethyl alcohol.

The X-ray powder diffraction (XRD) of Sn/Sn-*n*-C_4H_9, Sn/Si-*n*-C_4H_9, and Sn/SiO_2 are shown in Figure 1. In all samples, the first five identified peaks match the (200), (101), (220), (211), and (301) crystal planes of β-Sn.[20] However, both Sn/*n*-C_4H_9 and Sn/Si-*n*-C_4H_9 samples show additional peaks. In the XRD of Sn/*n*-C_4H_9, three very board peaks are seen at 20.6°, 33.8°, and 51.8°. These peaks match crystal plane of SnO_2 (JCDPS, 41-1445): (100), (101), and (211). The very broad width of these peaks is due to the very small size of these particles (<1 nm). The presence of nanocrys-

(20) See JCPDS 4-0673.

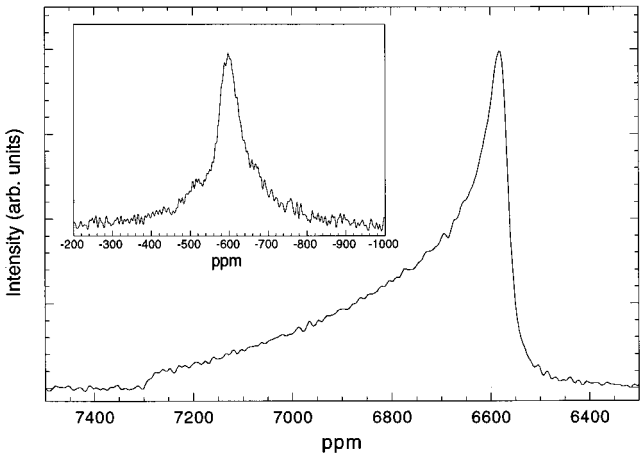

Figure 3. The ^{119}Sn spin-echo NMR spectrum of the Sn/SiO_2 sample. The inset shows the ^{119}Sn spin-echo MAS NMR spectrum (12.5 kHz spining rate) of the Sn−O region.

talline SnO_2 in the powder diffraction pattern suggests that the nanoclusters are not well terminated by the reaction with *n*-BuLi. In the XRD of the Sn/Si-*n*-C_4H_9 sample, additional diffraction peaks are present due to impurities and some can be assigned to either Si or SnO_2. The cleanest synthetic route appears to be for the Sn/SiO_2 nanoparticles that provides a diffraction pattern free of impurities, consistent with β-Sn. The average size for the Sn/SiO_2 samples, calculated from the Scherrer equation, ranged from 8 nm corresponding to short reflux times to 22 nm for samples with longer reflux times. XRD of the samples after several months were identical to the originals.

In the FTIR spectra for Sn/*n*-C_4H_9 and Sn/Si-*n*-C_4H_9 nanoparticles, shown in Figure 2, five characteristic peaks were observed, i.e., 2960, 2920, 2840, 1460, and 780 cm^{-1}. These peaks are assigned to terminal $-CH_3$ asymmetric stretching, $-CH_2$ asymmetric stretching, $-CH_2$ symmetric stretching, terminal $-CH_3$ bending, and terminal $-CH_3$ rocking.[21] These data are consistent with the *n*-butyl group terminating the surface, and there is no evidence of oxide. Crystalline SnO_2 gives a Sn−O absorption at 800−880 cm^{-1}. Nanocrystalline SnO_2 is expected to provide a very weak absorption due to the differences in local bonding, and there is a small peak at 770−800 cm^{-1} that might be attributed to Sn−O. FTIR spectrum for Sn/SiO_2 nanoparticles shows a peak from 1150 to 1000 cm^{-1}, a typical absorption for the Si−O stretch. Another two broad peaks, 3400−3000 and 1700−1500 cm^{-1}, are assigned to the O−H stretching frequency and overtone of water. The FTIR spectra do not change even after several months, suggesting that once prepared that the oxidation occurs in the synthesis step and does not continue to any appreciable extent over time.

Figure 3 shows the ^{119}Sn spin-echo NMR spectra of Sn/SiO_2. The static (nonspinning) ^{119}Sn NMR spectrum of the downfield region comprises a powder pattern due to the anisotropic Knight shift of tetragonal β-Sn. This spectrum is nearly identical to that previously reported for crystalline metallic tin.[22] The inset of Figure 3 shows the NMR region for SnO_2. There is a broad peak centered near −600 ppm with an intensity corresponding to 0.6 ± 0.2 mmol (oxide)/g (sample), indicating that the amount of SnO_2 is significant. The broad chemical shift distribution (66 ppm, fwhm with MAS) is characteristic of an amorphous phase; there is no evidence for crystalline SnO_2, which gives a very narrow peak (3 ppm fwhm) at −600 ppm. There are two possibilities to account for the amorphous SnO_2: one is that is due to unreacted starting material that have been oxidized after reaction and the other is that the SiO_2 surface is actually a mixed SnO_2/SiO_2 layer.

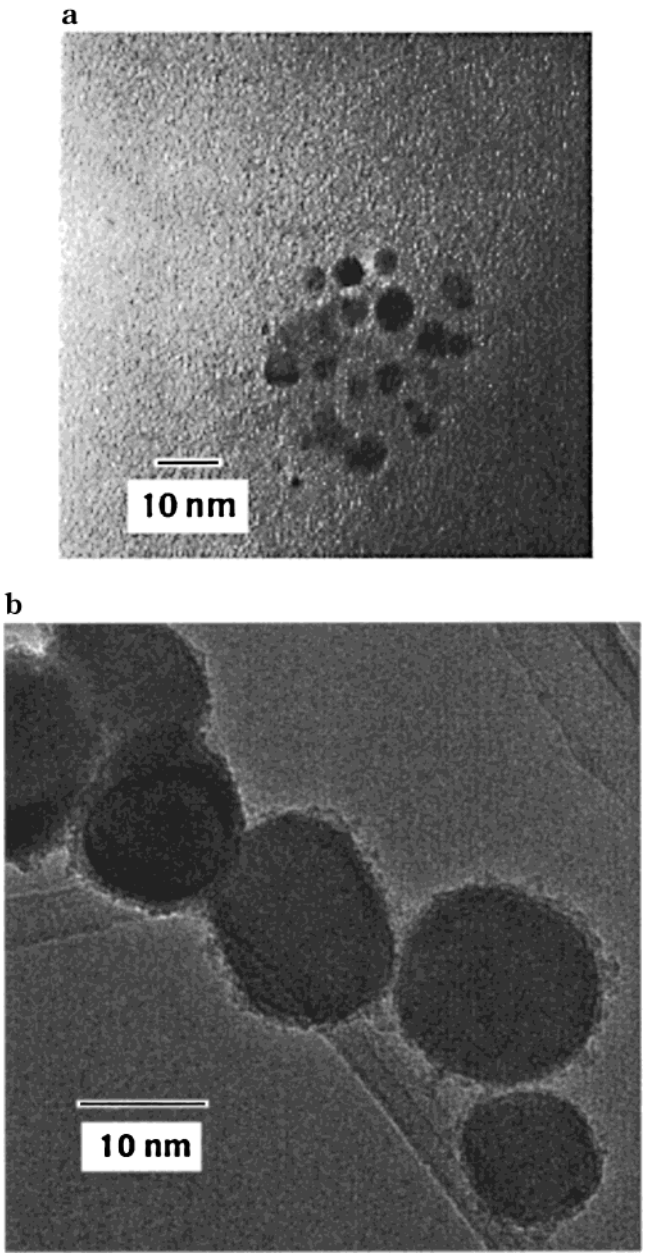

Figure 4. (a) A micrograph for Sn/*n*-C_4H_9 nanoparticles using a Top Con 002B TEM and (b) a micrograph for Sn/Si-*n*-C_4H_9 using a Philips CM 300 TEM.

TEM images of Sn/*n*-C_4H_9 and Sn/Si-*n*-C_4H_9 are shown in Figure 4a,b. The average sizes of Sn/*n*-C_4H_9 and Sn/Si-*n*-C_4H_9 nanoparticles (diameter) are 6.5 (1.7) and 8.7 (2.3) nm. Figure 4b clearly shows a nonuniform coating the surface of the nanoparticles. The selected area electron diffraction (SAED) shows only crystalline β-Sn without any additional diffraction, suggesting that

(21) Socrates, G. *Infrared Characteristic Group Frequencies*; Wiley: New York, 1980.
(22) Bloembergen, N.; Rowland, T. J. *Acta Metall. Sin.* **1953**, *1*, 731.

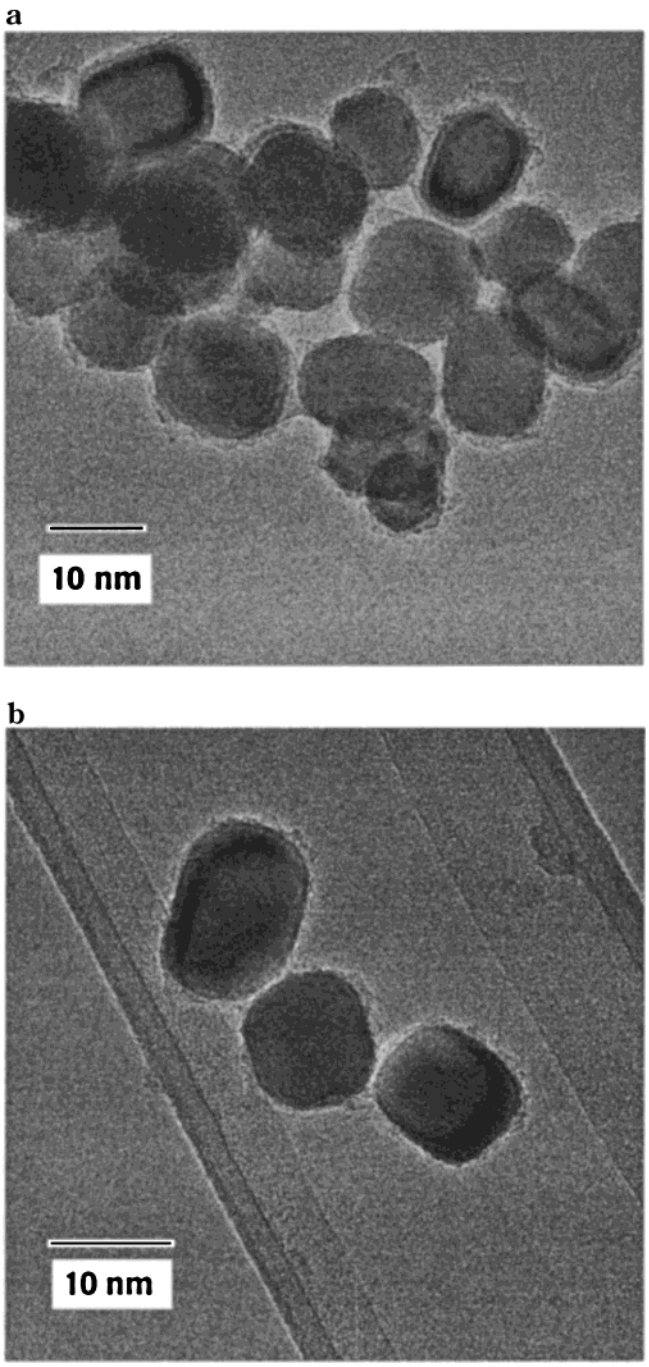

Figure 5. (a) A typical TEM image containing a part of a large number of Sn/SiO_2 nanoparticles and (b) different shapes of nanoparticles are shown in this image, such as cylinder, oval, rectangular, and cubic.

this coating is amorphous. A typical HRTEM image containing a large number of Sn/SiO_2 nanoparticles and showing some unusual shapes is shown in Figure 5a,b. In these micrographs, the capping of the SiO_2 sphere is clearly observed. These nanoparticles also display some interesting shapes, such as cylindrical, oval, rectangular, and cubic. The mechanism of the reaction that provides these morphologies is not clear. The reflux temperature, solvent, and the concentration of the starting reagents may play important roles here and need to be investigated further. The NMR shows a significant amount of amorphous SnO_2 that may also be contributing to the amorphous outer sphere. The average NMR chemical shift of the oxide region is

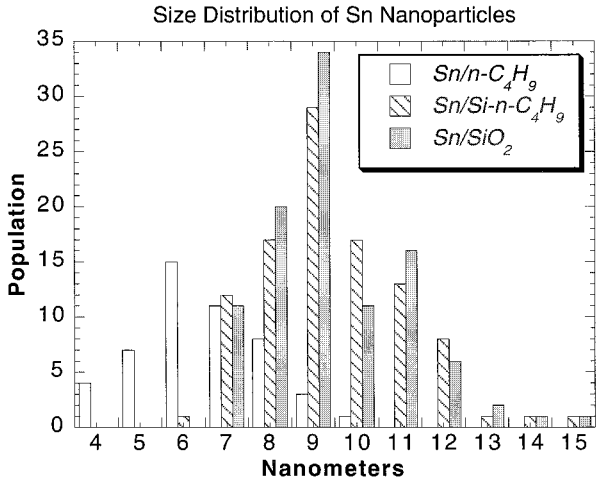

Figure 6. The histogram of size distribution for Sn/Sn and Sn/Si core/shell nanoparticles derived from seven TEM images. The average size is 9.41 nm with a standard derivation of 0.84 nm.

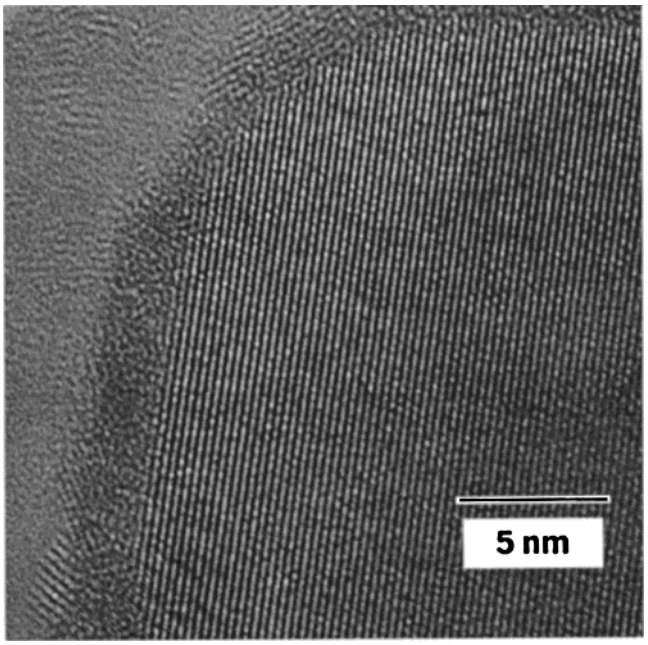

Figure 7. A view showing the interface between the core part and outer sphere of a Sn/SiO_2 nanoparticle. The Rr value varies from 0.181 (8 nm nanoparticle) to 0.102 (36 nm nanoparticle). The core part shows lattice fringes (2.92 Å) matching that of β-Sn (200). The nanoparticles contain polycrystalline core part (Sn) and amorphous outer sphere (SiO_2).

consistent with Sn in 6-coordination with oxygen, but a large amount of short-range disorder is indicated by the width of the observed peak which spans the entire chemical shift range for tin oxides. The NMR evidence is consistent with the presence of amorphous SnO_2, either present as an impurity or possibly the surface is a mixed SnO_2/SiO_2 amorphous layer. The average diameter for Sn/SiO_2 derived from seven TEM images is 9.41 (0.84) nm and the size distribution is shown in Figure 6. The radii ratio (Rr), the radius of the shell (SiO_2)/the radius of core (Sn), is obtained from TEM images. A close look at the interface between the core and the shell is shown in Figure 7. The d space of the lattice fringes of the core is 2.92 Å, matching the Sn crystal plane {200}. By comparing the seven TEM images of Sn/SiO_2, we found the capping thickness of

the amorphous layer to vary inversely with the size of nanoparticles. The Rr value is varied from 0.18 (8-nm particle) to 0.10 (36-nm particle). The average Rr value calculated from 24 individual nanoparticles, ranging in size from 6 to 12 nm, is 0.17 with a standard derivation of 0.02.

Summary

Sn/*n*-C_4H_9, Sn/Si-*n*-C_4H_9, and Sn/SiO_2 nanoparticles are prepared with the reaction of Mg_2Sn with $SnCl_4$ or $SiCl_4$ in glyme. The surface of these nanoparticles is terminated with *n*-butyl via *n*-butyllithium or further oxidized to silica by refluxing with 30% hydrogen peroxide. The X-ray powder diffraction patterns of these nanoparticles show the tetragonal structure of β-tin. The X-ray powder diffraction patterns of Sn/*n*-C_4H_9 and Sn/Si-*n*-C_4H_9 showed additional impurities, whereas Sn/SiO_2 was free of crystalline impurities. FTIR spectra provide supporting evidence for the termination of the *n*-butyl group on Sn/*n*-C_4H_9 and Sn/Si-*n*-C_4H_9 and SiO_2 layer on Sn/SiO_2 nanoparticles. The presence of a very weak, broad peak at 850−800 cm^{-1} in the FTIR is consistent with the presence of nanocrystalline and amorphous SnO_2 in the Sn/*n*-C_4H_9 and the Sn/SiO_2 samples, respectively. In the case of Sn/SiO_2, the presence of amorphous SnO_2 was detected by ^{119}Sn NMR, and it is possible that the outer sphere is a mixed SiO_2/SnO_2 layer. SAED is consistent with the result of XRD, indicating that the core part of the nanocluster is β-Sn. The TEM images show the shapes of nanoparticles are varied. The high contrast between SiO_2 and Sn make the measurement of the Rr value possible. The average Rr value for Sn/SiO_2 derived from TEM images is 0.17 (0.02). Further work is necessary to optimize the reaction parameters to provide a narrow size distribution and better control over the surface derivitization.

Acknowledgment. The authors are grateful to the National Science Foundation (grant DMR-9803074) and Campus Laboratory Collaboration Program of the University of California for financial support. Work at the NCEM was performed under the auspices of the director, Office of Energy Research, Office of Basic Energy Science, Materials Science Division, U.S. Department of Energy under Contract DE-AC-03-76-XF00098. The authors thank Dr. Young Chung Wang and Dr. Wen-Jauh Chen's very useful help and discussion in CM300 TEM. The authors thank the W.M. Keck NMR Laboratory (UC Davis) for the use of the solid-state NMR spectrometer.

CM990529Z